INFERENCE FOR DECORATED GRAPHS AND APPLICATION TO MULTIPLEX NETWORKS

Charles Dufour
Institute of Mathematics, Ecole Polytechnique Fédérale de Lausanne,
Station 8, 1015 Lausanne, Switzerland
charles.dufour@epfl.ch

Sofia C. Olhede
Institute of Mathematics, Ecole Polytechnique Fédérale de Lausanne,
Station 8, 1015 Lausanne, Switzerland
sofia.olhede@epfl.ch

August 20, 2024

ABSTRACT

A graphon is a limiting object used to describe the behaviour of large networks through a function that captures the probability of edge formation between nodes. Although the merits of graphons to describe large and unlabelled networks are clear, they traditionally are used for describing only binary edge information, which limits their utility for more complex relational data. Decorated graphons were introduced to extend the graphon framework by incorporating richer relationships, such as edge weights and types. This specificity in modelling connections provides more granular insight into network dynamics. Yet, there are no existing inference techniques for decorated graphons. We develop such an estimation method, extending existing techniques from traditional graphon estimation to accommodate these richer interactions. We derive the rate of convergence for our method and show that it is consistent with traditional non-parametric theory when the decoration space is finite. Simulations confirm that these theoretical rates are achieved in practice. Our method, tested on synthetic and empirical data, effectively captures additional edge information, resulting in improved network models. This advancement extends the scope of graphon estimation to encompass more complex networks, such as multiplex networks and attributed graphs, thereby increasing our understanding of their underlying structures.

Keywords Decorated Graph · Edge Attributed · Graphon · Inference · Multiplex Network

1 Introduction

Graphons have emerged as a fundamental tool in studying large, unlabelled simple networks, offering a robust framework grounded in the theory of exchangeability (Diaconis & Janson, 2007). These mathematical objects serve as the limiting objects for sequences of dense graphs and are instrumental in domains such as sociology, biology, and computer science, where understanding the asymptotic properties of large networks is crucial (Lovász, 2012). Traditional graphons encode binary information on edges, indicating the presence or absence of connections between nodes. However, many real-world networks exhibit richer structures, where edges carry additional information beyond mere connectivity, such as weights or types. For example, in a social network, edges between individuals might not only indicate friendship (a binary state) but also the frequency of interaction (a weight) or the type of relationship (colleague, friend, co-authorship) (Resnick et al., 1997; Magnani et al., 2013). In biological networks, edges might represent different biochemical interactions (e.g., protein-protein interactions, gene regulation), with decorations capturing the interaction strength or type. In transportation networks, edges can be decorated with travel time, cost, or type of transportation mode (e.g., bus, train, flight) (Cardillo et al., 2013).

To address these complexities, Lovász & Szegedy (2010) introduced the theoretical framework of decorated graphons (also called probability graphons (Abraham et al., 2023; Zucal, 2024)), which extend traditional graphons by allowing edges to carry more detailed information (decorations). Multiplex networks naturally fit into this framework (Kivelä et al., 2014); in multiplex networks, multiple types of connections can exist between the same set of nodes. By enumerating all possible combinations of these various connections and representing them as decorated edges, we can effectively treat multiplex networks as decorated graphs.

Significant advancements have been made in extending graph models to handle complex relational data, including graphs with attributes (Donier-Meroz et al., 2023; Chandna et al., 2022b; Su et al., 2020), time-varying networks (Chandna & Maugis, 2020; Pensky, 2019), and multilayer networks (Barbillon et al., 2017; Avrachenkov et al., 2022; Chandna et al., 2022a; Skeja & Olhede, 2024; Wang et al., 2024). Among others, Pensky (2024), Xu et al. (2020), and Fishkind et al. (2021) explore specific models that fit broadly within the framework of decorated graphons. Additionally, recent work by Lubberts et al. (2024) on edge-attributed graphs further expands our understanding by incorporating random line graphs into network inference, illustrating the ongoing evolution of graph modelling in increasingly complex contexts.

Our primary contribution is developing the first estimation method tailored for decorated graphons, to the best of our knowledge. This method extends the network histogram (Olhede & Wolfe, 2014) to accommodate the additional complexity of decorated edges and generalises the multiplex stochastic block model of Barbillon et al. (2017). By leveraging the properties of decorated graphons, we provide a comprehensive approach to infer the underlying generative mechanisms of complex networks. Our methodology preserves the rates of convergence of traditional graphon estimation (Gao et al., 2015; Klopp et al., 2017; Verdeyme & Olhede, 2024) and enhances its applicability to a wider array of network types.

2   Decorated graphs and graphons

We will start from a simple binary graph and build up to decorated graphs. A simple graph G is a pair (V, E), where V is a set of vertices (usually taken to be $[n] = \{1, \ldots, n\}$), and E is a set of unordered pairs of vertices called edges. The adjacency matrix $A \in \{0, 1\}^{n \times n}$ represents these edges, where $A_{ij} = 1$ if there is an edge between vertices i and j, and $A_{ij} = 0$ otherwise. This binary model effectively captures the presence or absence of links between nodes.

While traditional binary graphs capture simple connections, they fall short in representing more nuanced inter-node relationships. To address the limitations of the binary graph in capturing more complex and nuanced relationships, we introduce the concept of decorated graphs (Lovász & Szegedy, 2010). In this extended framework, each edge is not just binary but can carry additional information or 'decorations'. These decorations enrich the graph's structure by allowing edges to represent more than mere connections—they can include attributes like weights, interaction types, or other relevant properties. Decorated graphs are thus defined as complete simple graphs where each edge (i, j) is associated with an element from a set $\mathcal{K}$, which can be a finite set of colours, a set of weights, or any other finite categorisation that adds depth to the analysis of network interactions. These networks are also referred to as edge-attributed graphs in the literature.

More precisely, for $\mathcal{K}$ a set, a $\mathcal{K}$-decorated graph $\boldsymbol{G}$ is a complete simple graph where each edge (i, j) is decorated by an element of $\mathcal{K}$. Usually, $\mathcal{K}$ will have a special element $0_{\mathcal{K}}$, and the edges decorated by $0_{\mathcal{K}}$ will be considered missing. Similarly to simple graphs, such a graph can be represented by an adjacency matrix $\boldsymbol{A} \in \mathcal{K}^{n \times n}$. Requiring $\boldsymbol{G}$ to be exchangeable is equivalent to requiring $\boldsymbol{A}$ to be jointly exchangeable, i.e. $\{\boldsymbol{A}_{ij}\}$ and $\{\boldsymbol{A}_{\pi(i)\pi(j)}\}$ have the same distribution for every permutation π. We now focus on the generating mechanism of such $\mathcal{K}$-valued exchangeable arrays.

Definition 2.1 ($\mathcal{K}$-graphon (Lovász & Szegedy, 2010)) *Let $\mathcal{P}(\mathcal{K})$ denote the set of probability Borel measures on a compact space $\mathcal{K}$, and let $\mathcal{W}(\mathcal{K})$ denote the set of two-variable Borel measurable functions*

$$W : [0, 1]^2 \mapsto \mathcal{P}(\mathcal{K}), \text{ such that } W(x, y) = W(y, x) \text{ for every } (x, y) \in [0, 1]^2.$$

Elements of $\mathcal{W}(\mathcal{K})$ are referred to as $\mathcal{K}$-graphons or decorated graphons when $\mathcal{K}$ is implicit.

As for the simple graph case, we can get a functional representation of a $\mathcal{K}$-decorated graph; from Kunszenti-Kovács et al. (2022); Kallenberg (2005), we get that if $\mathcal{K}$ is a compact Hausdorff space and $\boldsymbol{A} \in \mathcal{K}^{n \times n}$ is jointly exchangeable, there exists a $\mathcal{K}$-graphon W such that

$$\boldsymbol{A}_{ij} \mid \xi_i, \xi_j \overset{\text{iid}}{\sim} W(\xi_i, \xi_j), \text{ where } \xi_i \overset{\text{iid}}{\sim} U[0, 1], \tag{1}$$

where $\boldsymbol{A}_{ij} \sim W(x, y)$ indicates that $\boldsymbol{A}_{ij}$ follows the probability distribution characterized by $W(x, y)$. The representation in eq. (1) resembles the Aldous-Hoover theorem in the case of simple graphs (Aldous, 1981; Hoover, 1979). Indeed, if $\mathcal{K} = \{0, 1\}$, $\boldsymbol{A}$ is equivalent to the usual adjacency matrix, and $W(\xi_i, \xi_j)$ corresponds to a Bernoulli distribution.

2.1   Finitely decorated graphs

From now on, we assume $\mathcal{K}$ is a finite set, such that $\mathcal{K} = \{x_1, \ldots, x_L\}$ with the cardinality $|\mathcal{K}| = L < \infty$. While it may appear restrictive initially, the assumption of finite decoration is quite versatile and applicable to many network structures. For instance, weighted graphs, where the weights are discretized, naturally fit the model of finitely decorated graphs. Furthermore, multiplex networks, characterised by multiple types of connections between the same pair of vertices, can also be effectively described within this framework. By treating each unique combination of edge types between two nodes as a distinct decoration, we can capture the complexity of multiplex networks as finitely decorated graphs. The utility of finitely decorated graphs extends further into several other mathematical constructs that benefit from this rich structural definition. For example, coloured graphs, where edges are assigned colours from a finite palette, seamlessly translate into finitely decorated graphs when each colour represents a specific type of connection or property.

To establish a probability distribution over $\mathcal{K}$, it is sufficient to define L probabilities. Accordingly, a $\mathcal{K}$-graphon W is characterised by L symmetric measurable functions $w^{(l)} : [0,1]^2 \rightarrow [0,1]$, where the sum over all functions at any pair (x,y) equals 1, i.e., $\sum_l w^{(l)}(x,y) = 1$; here $w^{(l)}$ represents the probability of realisation of the lth decoration x_l. Given fixed $x, y \in [0,1]$, $W(x,y)$ corresponds to an element of the set $\{p \in [0,1]^L : \|p\|_1 = 1\}$ (Lovász & Szegedy, 2010). When conditioned on the latent variables $\{\xi_i\}$, we define:

$$\boldsymbol{\theta}_{ij} = W(\xi_i, \xi_j) \text{ for } i, j \in [n],$$

where $\boldsymbol{\theta}_{ij} \in [0,1]^L$. The subsequent section outlines the method for estimating W from a single realisation $\boldsymbol{A} \in \mathcal{K}^{n \times n}$.

3   Inference of finitely decorated graphons

In this section, we introduce the methodology for estimating finitely decorated graphons, expanding the capabilities of traditional graph analysis tools. Piece-wise constant functions have been used to approximate smooth graphon for simple graphs (Wolfe & Olhede, 2013; Gao et al., 2016; Janson & Olhede, 2021). We will show that the same can be done for decorated graphons. To do so, we extend the class of stochastic shape models of Verdeyme & Olhede (2024). The stochastic shape model is an extension of the traditional block model. Both are piece-wise constant functions; the pieces for the block model are assumed to be squares, while the shape model relaxes this assumption by allowing multiple squares to be combined into a single shape, thus reducing the number of parameters (see fig. 1).
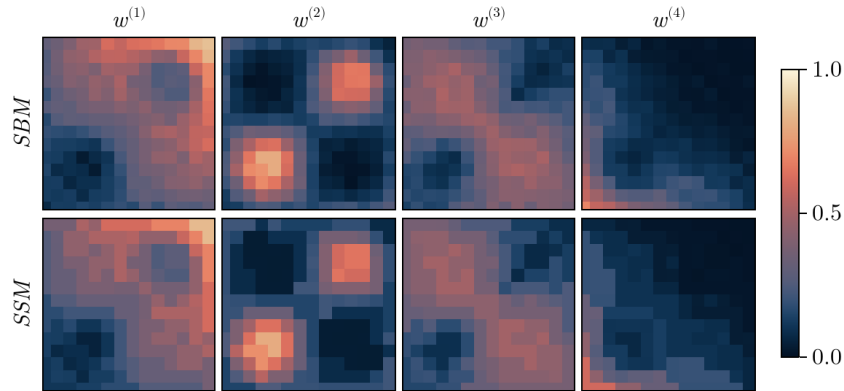

Figure 1: Stochastic Block Model approximation (SBM) of W_3 (see section 5) in the first row and estimated decorated graphon using a decorated $(s = 27, k = 14)$-Stochastic Shape Model (SSM) in the second. The smoothing effect of using shapes instead of blocks is particularly visible in $w^{(4)}$ on the right-hand side. The estimator was computed based on an observation with 300 nodes.

Definition 3.1 ($\mathcal{K}$-decorated (s,k)-Stochastic Shape Model (SSM)) *Let $|\mathcal{K}| = L$. Assume we have defined $s \in \mathbb{N}^+$ symmetric regions in $[0,1]^2$ that are unions of blocks of length k^{-1}. Let $z : [n] \times [n] \rightarrow s$ be the symmetric mapping from a pair of nodes to its associated shape index. We can then define the function W for the s constants $\boldsymbol{\theta}_c$, to be*

$$W(x,y) = \boldsymbol{\theta}_{z(x,y)} \in [0,1]^L.$$

There are two approaches when it comes to graphon estimation. We can estimate the point-wise distribution of the decorations, i.e. estimating $\boldsymbol{\theta}_{ij} = W(\xi_i, \xi_j)$. Alternatively, we may want to recover the continuous graphon over its whole domain $[0,1]^2$.

For the point-wise estimation, we consider the following mean squared error loss

$$\frac{1}{n^2} \sum_{i,j \in [n]} \|\widehat{\boldsymbol{\theta}}_{ij} - \boldsymbol{\theta}_{ij}\|_2^2 = \frac{1}{n^2} \sum_{i,j \in [n]} \sum_{l \in [L]} \left(\widehat{\boldsymbol{\theta}}_{ij}^{(l)} - \boldsymbol{\theta}_{ij}^{(l)}\right)^2 = \frac{1}{n^2} \|\widehat{\boldsymbol{\theta}} - \boldsymbol{\theta}\|_F^2, \tag{2}$$

where $\widehat{\boldsymbol{\theta}}$ is an estimator of $\boldsymbol{\theta}$ and $\|\cdot\|_F$ is the Frobenius norm. This loss is appropriate for estimating the matrix $\boldsymbol{\theta}$ induced by W (Gao et al., 2016). In simple binary networks, each edge is modelled as a Bernoulli random variable $A_{ij} \sim \text{Bern}(\theta_{ij})$. In that case, maximising the likelihood is equivalent to minimising the mean squared error $\|A - \theta\|_2^2 = \sum_{i,j} (A_{ij} - \theta_{ij})^2$ as explained by Gao et al. (2016); Wolfe & Olhede (2013) and Gaucher & Klopp (2021a). For decorated graphs, a direct comparison using least squares between observed $\boldsymbol{A}_{ij}$ and probabilities $\boldsymbol{\theta}_{ij}$ is not feasible, as the former lies in $\mathcal{K}$ and the later lies in $[0,1]^L$. To address this, we transform $\boldsymbol{A}_{ij}$ into a single-entry binary vector $\boldsymbol{X}_{ij} \in \{0,1\}^L$, where each dimension reflecting the activation or non-activation of each defined edge type within $\mathcal{K}$ (see appendix A for a more precise statement). In particular, the expectation of $\boldsymbol{X}_{ij}$ under the model is $\boldsymbol{\theta}_{ij}$. We can now define our estimator as the solution to the following least-squares problem

$$\widehat{\boldsymbol{\theta}} = \underset{\boldsymbol{\theta} \in \Theta_{s,k}}{\arg\min} \frac{1}{n^2} \|\boldsymbol{X} - \boldsymbol{\theta}\|_F^2, \tag{3}$$

where $\Theta_{s,k}$ is the set of $n \times n$ parameter matrices from a (s,k)-stochastic shape model. One can show that this is equivalent to finding an optimal partition of the nodes and edges (Verdeyme & Olhede, 2024).

Estimating the graphon function adds a layer of complexity as it is closely related to non-parametric regression with unknown design (Gao et al., 2016). The exchangeability assumption implies that a decorated graphon W and $W_\sigma(x,y) := W(\sigma(x), \sigma(y))$ define the same probability distribution on decorated graphs for $\sigma : [0,1] \to [0,1]$ a measure-preserving bijection. Following Olhede & Wolfe (2014), we consider the Mean Integrated Square Error (MISE) to estimate W as a continuous function:

$$\inf_{\sigma \in \mathcal{M}} \iint_{(0,1)^2} \sum_{l \in [L]} \left(W_\sigma^{(l)}(x,y) - \widehat{W}^{(l)}(x,y)\right)^2 dx\,dy = \inf_{\sigma \in \mathcal{M}} \iint_{(0,1)^2} \left\|W^\sigma(x,y) - \widehat{W}(x,y)\right\|_2^2 dx\,dy,$$

where $\mathcal{M}$ is the set of all measure-preserving bijection from $[0,1]$ to $[0,1]$, and $\widehat{W}$ is an estimator of W. We will define our estimator of W as the discretized graphon based on $\widehat{\boldsymbol{\theta}}$ defined in eq. (3):

$$\widehat{W}(x,y) = W_{\widehat{\boldsymbol{\theta}}}(x,y) = \widehat{\boldsymbol{\theta}}_{\lceil nx \rceil, \lceil ny \rceil}. \tag{4}$$

4 Properties of estimator

We now study the property of the least squares estimator as defined in eq. (3) under settings similar to what is found in the current literature (Olhede & Wolfe, 2014; Gao et al., 2015; Klopp et al., 2017; Verdeyme & Olhede, 2024).

Assumption 1 *The decoration space $\mathcal{K}$ is a finite set, denoted as $|\mathcal{K}| = L < \infty$, $\mathcal{K} = \{x_1, \ldots, x_L\}$.*

Theorem 4.1 *Let W be a $\mathcal{K}$-decorated (s,k)-stochastic shape model, then for any $C' > 0$ there exists $C > 0$ such that*

$$\frac{1}{n^2} \sum_{i,j \in [n]} \left\|\widehat{\boldsymbol{\theta}}_{ij} - \boldsymbol{\theta}_{ij}\right\|_2^2 \leq C \left(\frac{sL}{n^2} + \frac{\log(\max(k,s))}{n}\right),$$

with probability at least $1 - \exp\left(-C'n \log s\right)$ uniformly over $\boldsymbol{\theta} \in \Theta_{s,k}$. Furthermore, we have

$$\sup_{\theta \in \Theta_{s,k}} \mathbb{E}\left[\frac{1}{n^2} \sum_{ij} \|\widehat{\boldsymbol{\theta}}_{ij} - \boldsymbol{\theta}_{ij}\|_2^2\right] \leq C_1 \left(\frac{sL}{n^2} + \frac{\log(\max(k,s))}{n}\right)$$

with some universal constant $C_1 > 0$ and $n > \max\left(0, k^2 - s\right)$.

This error comprises the non-parametric rate sL/n^2 and the clustering rate $\log(\max(k,s))/n$. The clustering rate is identical to what is found in the simple graph case (Gao et al., 2016). This is unsurprising as we are still facing the same clustering problem of finding an optimal partition of n nodes. Conversely, the change in the non-parametric rate reflects the change in our modelling assumptions: we now estimate not one but L parameters per shape.

Similarly, if W is Holder continuous with exponent α (assumption 2), we retrieve the usual non-parametric rates for simple graphons (Gao et al., 2016; Verdeyme & Olhede, 2024).

	W_1	W_2	W_3
$w^{(1)}(x,y)$	$(1-\min(x,y))(1-|x-y|)$	$\propto \sqrt{|x-y|}$	$\propto 3xy$
$w^{(2)}(x,y)$	$|x-y|(1-\min(x,y))$	$\propto \exp(-0.5|x-y|)$	$\propto 3\sin(2\pi x)\sin(2\pi y)$
$w^{(3)}(x,y)$	$\min(x,y)(1-|x-y|)$	$\propto \min(x,y)$	$\propto \exp\left(-3(x-0.5)^2+(y-0.5)^2\right)$
$w^{(4)}(x,y)$	$\min(x,y)|x-y|$	$\propto \exp(-\min(x,y)^{3/4})$	$\propto 2-3(x+y)$

Table 1: The table shows the decorated graphon parameters used for the simulations. W_2, W_3 are normalised to ensure a proper probability distribution. W_2 by the sum over decorations and W_3 using a softmax transformation.

Assumption 2 *The $\mathcal{K}$-decorated graphon W is Hölder continuous with exponent $\alpha \in (0,1]$, i.e.*

$$W \in \mathcal{H}(\alpha,M) \Leftrightarrow \sup_{(x,y)\neq(x',y')\in(0,1)^2} \frac{\|W(x,y)-W(x',y')\|_1}{\|(x,y)-(x',y')\|_1^\alpha} \leq M < \infty.$$

Theorem 4.2 *If $W \in \mathcal{H}(\alpha,M)$,*

$$\frac{1}{n^2}\sum_{ij}\|\widehat{\boldsymbol{\theta}}_{ij}-\boldsymbol{\theta}_{ij}\|_2^2 = O_p\left(n^{-2\alpha/(\alpha+1)}+\frac{\log(n)}{n}\right),$$

and

$$\inf_{\sigma\in\mathcal{M}}\iint_{(0,1)^2}\left\|W^\sigma(x,y)-\widehat{W}(x,y)\right\|_2^2 \mathrm{d}x\,\mathrm{d}y = O_p\left(n^{-2\alpha/(\alpha+1)}+\frac{\log(n)}{n}+n^{-\alpha\wedge 1}\right).$$

For a more detailed version of the results in this section and their proofs, see the appendix (theorem B.1 and proposition B.1). When $\mathcal{K}=\{0,1\}$, $L=2$, we can verify that the rates are identical to those of (Verdeyme & Olhede, 2024; Tsybakov, 2009). Donier-Meroz et al. (2023) considered graphons for weighted graphs focused on mean estimation, while here we characterise the whole distribution of the decorations.

5   Numerical experiments

In this section, we showcase the performance of our method by evaluating the Mean Squared Error (MSE) defined in eq. (2) between true and estimated decorated graphons. We consider the three cases described in section 5: W_1 and W_3 are Hölder smooth with $\alpha = 1$, while W_2 is Hölder continuous with $\alpha = 0.5$. We consider $n = \{300, 500, \ldots, 1900\}$ and run 10 simulation trials. More specifically, for a fixed n and $W \in \{W_1, W_2, W_3\}$, for each repetition we draw $\xi_i \sim U[0,1]$ for $i = 1,\ldots,n$ and $A_{ij} \sim W(\xi_i, \xi_j)$. We then estimate the $\boldsymbol{\theta}_{ij}$ matrix for each repetition with a (s,k)-stochastic shape model with $k = \lceil n^{1/(\alpha+1)} \rceil$ as dictated by theorem B.1 and starting from a spectral clustering as in Olhede & Wolfe (2014). Figure 2 shows that the errors behave according to our theory for n big enough (see theorems 4.1 and 4.2).
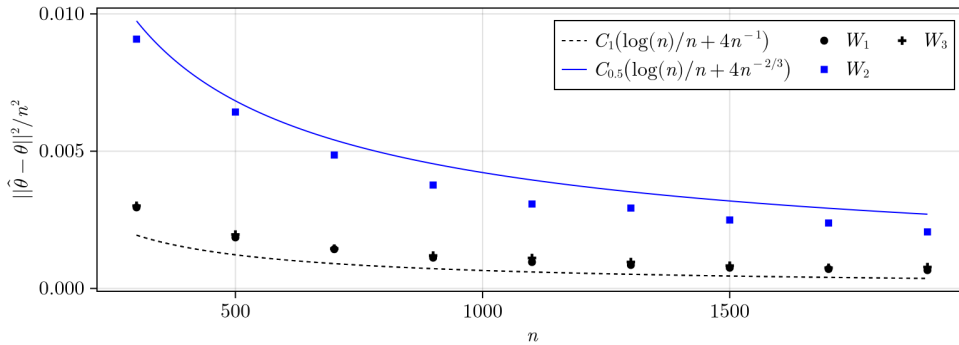

Figure 2: The MSE error of our block-estimator with for the independent W_1 and dependent layer W_3 case (see section 5 for more details). Each point represents the average of MSE over 10 independent repetitions, and the standard errors were of the order of 10^{-5}. The constants C_1, $C_{0.5}$ were picked for visibility.

Any multiplex network with a finite number of layers can be seen as a finitely decorated graph (Kivelä et al., 2014). Consider a multiplex network comprising n common nodes across T layers. We recast a multiplex network as a

$\{0,1\}^T$-decorated graph where $A_{ij}^{(t)} = A_{ji}^{(t)} = 1$ if there exists an edge between nodes i and j in layer t. We fix $T = 2$ and enumerate the different decorations $\mathcal{K} = \{[0,0], [1,0], [0,1], [1,1]\} = \{x_1, x_2, x_3, x_4\}$. This is an extension of the multiplex stochastic block model of Barbillon et al. (2017) to more complex connectivity surfaces. With this interpretation, we can see that W_1 is the decorated graphon for a 2-layer multiplex network with independent layers and marginal probabilities $\min(x, y)$ and $|x - y|$. On the other hand, W_2 and W_3 encode dependencies across the layers as the probabilities of the bivariate Bernoulli decorations cannot be written as a product of the marginal probabilities. Figure 2 shows that our method is equally effective at handling dependent and independent layers. For bivariate Bernoulli random variables, we can alternatively parameterise its distribution using the two marginals and the correlation (Teugels, 1990). We use this parametrization to visualise the estimated $\widehat{W_3}$ for different numbers of nodes in fig. 3.
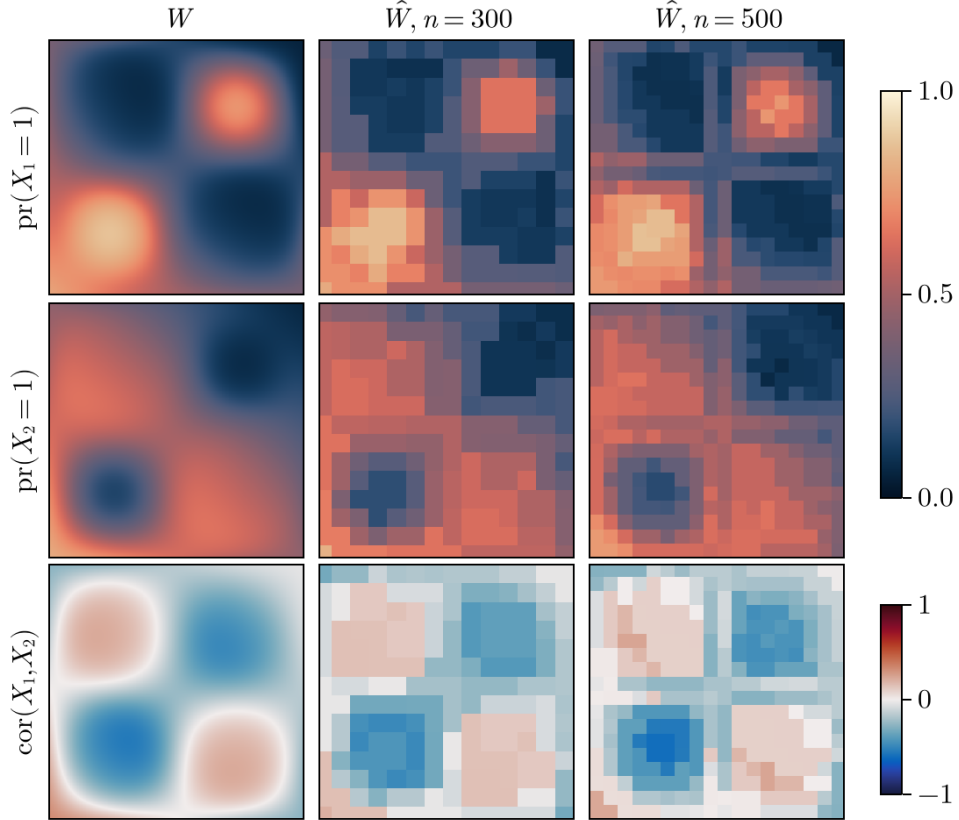

Figure 3: Ground truth W_3 (see section 5) in the first column. The two columns on the right show the presented estimator with increasing nodes observed.

6 Data Analysis

6.1 Multiplex of human diseases

Our decorated graphon model is applied to analyse a comprehensive dataset of 779 diseases, revealing intricate genetic and symptomatic relationships discussed by Halu et al. (2019). The multiplex network comprises of a genotype and phenotype layer where nodes represent diseases. Diseases are linked in the phenotype layer if they share a common symptom, and in the genotype layer, if linked to a common gene. The original dataset reports the number of connections as weight in each layer: in the genotype (phenotype) layer, only 130 (330) pairs of diseases have a weight of more than 1. We binarize these weighted adjacency matrices by keeping only one edge with a weight greater or equal to 1. To reduce the sparsity of the network, we keep the diseases with a degree of at least 2 in each layer, resulting in a multilayer graph with 204 diseases represented in the left-hand side of fig. 4. The range of the estimated correlation being mostly positive aligns with the authors' finding that diseases with common genetic constituents tend to share symptoms.
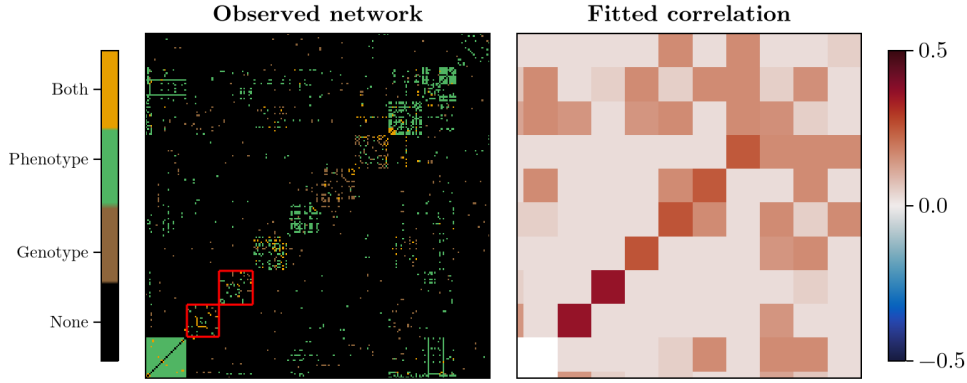
Figure 4: Visual Representation of the Multiplex Network of Human Diseases: This figure displays an ordered matrix of the network, organised by the refined categorisations derived from our decorated graphon estimation method, illustrating clearer patterns of disease interrelations. Fitted correlation matrix between the two layers on the right.

The second group forms a clique in the phenotype layer, leading to an estimated probability of connection of 1. This group includes diseases primarily affecting the nervous system and muscle function, such as Charcot-Marie-Tooth disease and spinocerebellar ataxia, indicating possible commonalities in genes affecting neuronal and muscular degeneration or dysfunction, and is a subset of the largest community outlined in Halu et al. (2019).

Groups 3 and 4 (highlighted within fig. 4 by a red square; see the supplemental material for more details) display a maximum correlation coefficient of 0.37 among the groups analysed. Cluster 3 contains diseases such as various forms of amyotrophic lateral sclerosis (ALS), Frasier syndrome, Gerstmann-Straussler-Scheinker syndrome, and metabolic conditions like obesity and X-linked hypophosphatemia. The shared characteristic among these diseases appears to be their primary impact on neurological function and, in some cases, metabolic dysregulation. For instance, different forms of ALS, despite having various specific genetic mutations, all typically involve neurodegenerative processes that might be traced back to shared or functionally similar genetic pathways. This aligns with the observed overlap in disease-disease interactions in the genotype and phenotype layers of the network studied in the paper, which supports the hypothesis that diseases with shared genetic underpinnings often manifest similar phenotypic characteristics.

Cluster 4 includes a variety of disorders with apparent and complex genetic roots such as ACTH-secreting pituitary adenomas and different syndromic presentations. According to the multiplex network analysis from Halu et al. (2019), diseases with similar clinical manifestations often share underlying molecular pathways, even if they initially appear disparate. The grouping in Cluster 4, which includes diseases like Klippel-Feil syndrome and syndactyly, likely represents a commonality in developmental genes or pathways affecting morphogenesis. This would suggest that such a cluster represents a biologically cohesive group where the diseases share more than just symptomatic similarities but also underlying genetic associations

6.2 High School contact network

We demonstrate differences between our approach and the classical graphon estimation methods by analysing a student contact network of 327 students, detailed in Mastrandrea et al. (2015). The study utilised various methods to assess contact patterns, including wearable sensors, contact diaries, friendship surveys, and online social networks. The data was collected within 9 classes divided into 4 specialisations. There are three classes each in Biology (BIO) and Mathematics and Physics (MP), two in Physics and Chemistry (PC), and one focused on Engineering studies (PSI). Over a period of 5 days, students wore sensors that recorded face-to-face interactions every 20 seconds during school hours. Additionally, friendship surveys and Facebook network data were used to enrich the dataset. We integrated these diverse data sources into a 3-layer multiplex network with binary edges, where each layer encoded one type of interaction. For the contact recorded by the wearable sensors, we recorded it in the corresponding layer as 1 if two students interacted for more than 100 seconds over the 5 days. The friendships and Facebook connections are already binary and thus can be incorporated as is. Figure 5 show the marginal probabilities of connection in each layer. Notice how we retrieve the similarity between the different classes and specialisations, which is expected (Mastrandrea et al., 2015).
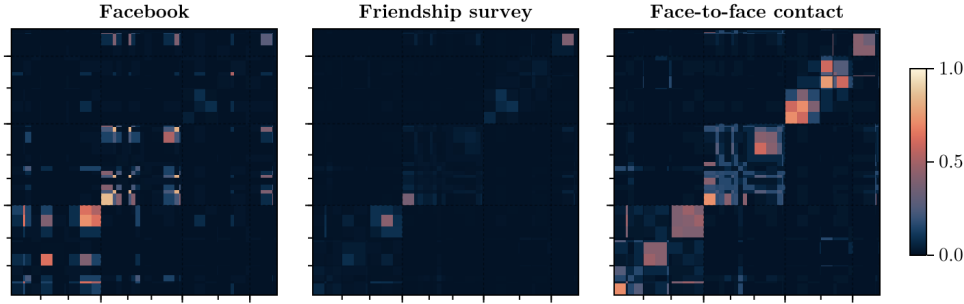
Figure 5: Marginal probability of having a certain connection between two students based on our fitted model. The data was sorted first by the class of the students and then by the grouping from the estimator. Notice how we retrieve the similarity between the different classes (indicated by the ticks) and specialisations (dashed lines).

Figure 6 showcases the advantage of our method compared to the simple graphon estimation. We can incorporate different connections, revealing a more subtle structure in the network. We fitted the Network Histogram (Olhede & Wolfe, 2014) to the network consisting of only the face-to-face contacts (the third layer in the multiplex). The left-hand side of fig. 6 shows the resulting fit of the network histogram, and we can see that the group and structure of the network unsurprisingly mostly follow the classes of the student. On the other hand, our method detects different sub-communities within classes. The method also seems to detect groups of students that interact with the other classes in the same specialities. We hypothesise that this may be the students retaking some years. However, since this data is unavailable, we could not verify this claim. If the dataset was collected for studying the epidemiology of infectious diseases, these sub-communities might be useful to show contact patterns outside of school hours. This might be a first step in overcoming the limitations of the space constraints of face-to-face recordings by incorporating more connections than just face-to-face contacts.
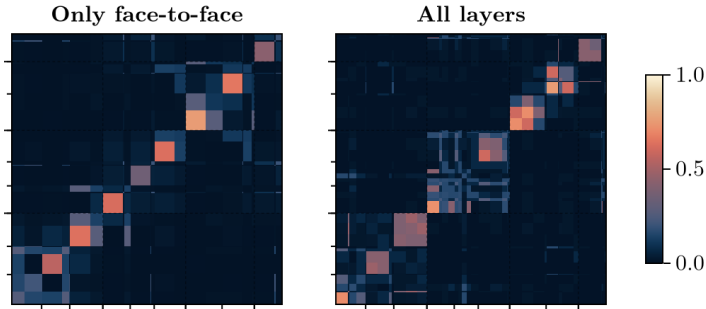

Figure 6: Estimated face-to-face contact probability, estimated from only the face-to-face contact data vs considering the joint information of the multilayer. Additional layers allow for a finer resolution than just the classes considered.

Acknowledgement

Supplementary material

Supplementary material includes additional simulation results, the proofs of theorems 4.1 and 4.2 and proposition B.1 and further results on the data analysis. All simulation results and figures can be reproduced in `Julia v1.10.3` (Bezanson et al., 2017) using the code available at `https://github.com/dufourc1/multiplex_limit.jl`. The method is implemented in the `NetworkHistogram.jl` package (Dufour & Grainger, 2023).

A Transformation

We define $\boldsymbol{X}_{ij}$ more precisely. Let $\boldsymbol{X}_{ij} \in \{0,1\}^L$ such that its lth coordinate $\boldsymbol{X}_{ij}^{(l)} = 1$ if $\boldsymbol{A}_{ij} = x_l \in \mathcal{K}$ and 0 otherwise. This defines a bijection between $\mathcal{K}$ and $\{a \in \{0,1\}^L : \|a\|_1 = 1\}$. For a $p \in [0,1]^L$ with $\|p\|_1 = 1$, we say that $X \sim \text{Multinoulli}(p)$ if its joint probability mass function is $\text{pr}(x) = \prod_l p_l^{x_l}$ if $x \in \{a \in \{0,1\}^L : \|a\|_1 = 1\}$ and 0 otherwise. Observing $\boldsymbol{A}$ as specified in eq. (1) is equivalent to observing $\boldsymbol{X}_{ij} \mid \boldsymbol{\xi} \overset{\text{iid}}{\sim} \text{Multinoulli}(\boldsymbol{\theta}_{ij})$, where $\boldsymbol{\theta}_{ij} \in [0,1]^L$ is the vector of probabilities representing the distribution $W(\xi_i, \xi_j)$. The advantage is that the distribution of $\boldsymbol{X}_{ij}$ is fully determined by its expectation $\mathbb{E}\left[\boldsymbol{X}_{ij} \mid \boldsymbol{\xi}\right] = \boldsymbol{\theta}_{ij}$.

B Technical details of the rate of convergence

The following theorem and proposition are the detailed version of theorem 4.2 and extend the results of Verdeyme & Olhede (2024); Gao et al. (2016) to the finitely decorated graphon case. The proofs can be found in the supplemental material.

Theorem B.1 *For $W \in \mathcal{H}(\alpha, M)$, $n > L$, there exists a constant $\beta \geq 1$ such that for any $C' > 0$, there exists a constant $C > 0$ only depending on C', M, α and β, where the following holds*

$$\frac{1}{n^2} \sum_{ij} \|\widehat{\boldsymbol{\theta}}_{ij} - \boldsymbol{\theta}_{ij}\|_2^2 \leq C \left(L n^{-2\alpha/(\alpha+1)} + \frac{\log(n)}{n} \right),$$

with probability at least $1 - \exp(-C'n)$, with $s = \left\lceil n^{\frac{2\beta-1}{\alpha \wedge 1 + 1}} \right\rceil$ and $k = \lceil n^{1/(\alpha+1)} \rceil$. Furthermore,

$$\sup_{W \in \mathcal{H}(\alpha, M)} \mathbb{E}\left[\frac{1}{n^2} \sum_{i,j \in} \|\widehat{\boldsymbol{\theta}}_{ij} - \boldsymbol{\theta}_{ij}\|_2^2 \right] \leq C_1 \left(L n^{-2\alpha/(\alpha+1)} + \frac{\log(n)}{n} \right),$$

for some other constant $C_1 > 0$ only depending on M. Both the probability and the expectation are jointly over $\{\boldsymbol{A}_{ij}\}$ and $\{\xi_i\}$.

Proof B.1 (of theorem B.1) *See the supplemental material.*

Proposition B.1 *For $W \in \mathcal{H}(\alpha, M)$, $n > L$, there exists a constant $\beta \geq 1$ such that for any $C' > 0$, there exists a constant $C > 0$ only depending on C', M, α and β, where the following holds*

$$\text{MISE}\left(\widehat{W}_{\widehat{\boldsymbol{\theta}}}, W\right) \leq C \left(L n^{-2\alpha/(\alpha+1)} + \frac{\log(n)}{n} + n^{-\alpha \wedge 1} \right),$$

with probability at least $1 - \exp(-C'n)$, with $s = \left\lceil n^{\frac{2\beta-1}{\alpha \wedge 1 + 1}} \right\rceil$ and $k = \lceil n^{1/(\alpha+1)} \rceil$. Furthermore,

$$\sup_{W \in \mathcal{H}(\alpha, M)} \mathbb{E}\left[\text{MISE}\left(\widehat{W}_{\widehat{\boldsymbol{\theta}}}, W\right) \right] \leq C_1 \left(L n^{-2\alpha/(\alpha+1)} + \frac{\log(n)}{n} + n^{-\alpha \wedge 1} \right),$$

for some other constant $C_1 > 0$ only depending on M. Both the probability and the expectation are jointly over $\{\boldsymbol{A}_{ij}\}$ and $\{\xi_i\}$.

Proof B.2 (of proposition B.1) *Klopp et al. (2017) showed that the mean integrated error is bounded by*

$$\mathbb{E}\left[\text{MISE}\left(\widehat{W}_{\widehat{\boldsymbol{\theta}}}, W\right) \right] \leq 2 \underbrace{\mathbb{E}\left[\frac{1}{n^2} \left\|\widehat{\boldsymbol{\theta}} - \boldsymbol{\theta}\right\|_F^2 \right]}_{\text{estimation error}} + 2 \underbrace{\mathbb{E}\left[\text{MISE}\left(W_{\boldsymbol{\theta}}, W\right) \right]}_{\text{agnostic error}},$$

where the agnostic error is the distance between the true graphon and its discretized version sampled at the unknown $\{\xi_i\}$. A direct adaptation of Klopp et al. (2017, Prop. 3.5) shows that the agnostic error is bounded by $n^{-\alpha \wedge 1}$, which leads to

$$\sup_{W \in \mathcal{H}(\alpha, M)} \mathbb{E}\left[\text{MISE}\left(\widehat{W}_{\widehat{\boldsymbol{\theta}}}, W\right) \right] \leq C_2 \left(n^{-2\alpha/(\alpha+1)} + \frac{\log(n)}{n} + n^{-\alpha \wedge 1} \right), \tag{5}$$

where we use theorem B.1 to bound the estimation error.

C   Optimisation: practical consideration

The results presented in section 4 are valid for a global optimum of eq. (3). This problem boils down to finding an optimal partition of the vertices, which is, in principle, NP-hard. We approximate this global optimum using a greedy label-switching algorithm (Bickel & Chen, 2009; Olhede & Wolfe, 2014). The starting point of this label-switching algorithm can influence whether we end up in a local optimum, but picking a good starting point (e.g. spectral clustering (Olhede & Wolfe, 2014; Arroyo et al., 2021)) instead of a random one helps to reduce the optimality gap in practice.

Remark C.1 *Barbillon et al. (2017) use variational inference (Celisse et al., 2012) to fit the multiplex stochastic block model, while our code (Dufour & Grainger, 2023) uses least-squares. Gaucher & Klopp (2021a,b) discuss the relationship between the two estimators and show that both are minimax optimal in the context of traditional graphon estimation.*

To decide the resolution k when α is unknown, we use the automatic bandwidth estimation of Olhede & Wolfe (2014) on each decorations probabilities $w^{(l)}$ yielding $\hat{k}_l$, and pick the biggest group number $\hat{k} = \max_l \hat{k}_l$. This is equivalent to taking the least regular $w^{(l)}$ to decide the number of groups needed. The number of shapes s is picked using the Bayesian Information Criterion (BIC) as in Verdeyme & Olhede (2024).

References

ABRAHAM, R., DELMAS, J.-F. & WEIBEL, J. (2023). Probability-graphons: Limits of large dense weighted graphs. ArXiv:2312.15935 [cs, math].

ALDOUS, D. J. (1981). Representations for partially exchangeable arrays of random variables. *Journal of Multivariate Analysis* **11**, 581–598. Publisher: Elsevier.

ARROYO, J., ATHREYA, A., CAPE, J., CHEN, G., PRIEBE, C. E. & VOGELSTEIN, J. T. (2021). Inference for Multiple Heterogeneous Networks with a Common Invariant Subspace. *Journal of Machine Learning Research* **22**, 1–49.

AVRACHENKOV, K., DREVETON, M. & LESKELÄ, L. (2022). Community recovery in non-binary and temporal stochastic block models. ArXiv:2008.04790 [cs, math, stat].

BARBILLON, P., DONNET, S., LAZEGA, E. & BAR-HEN, A. (2017). Stochastic Block Models for Multiplex Networks: An Application to a Multilevel Network of Researchers. *Journal of the Royal Statistical Society Series A: Statistics in Society* **180**, 295–314.

BEZANSON, J., EDELMAN, A., KARPINSKI, S. & SHAH, V. B. (2017). Julia: A Fresh Approach to Numerical Computing. *SIAM Review* **59**, 65–98. Publisher: Society for Industrial and Applied Mathematics.

BICKEL, P. J. & CHEN, A. (2009). A nonparametric view of network models and Newman–Girvan and other modularities. *Proceedings of the National Academy of Sciences* **106**, 21068–21073. Publisher: National Acad Sciences.

CARDILLO, A., GÓMEZ-GARDEÑES, J., ZANIN, M., ROMANCE, M., PAPO, D., POZO, F. D. & BOCCALETTI, S. (2013). Emergence of network features from multiplexity. *Scientific Reports* **3**, 1344. Publisher: Nature Publishing Group.

CELISSE, A., DAUDIN, J.-J. & PIERRE, L. (2012). Consistency of maximum-likelihood and variational estimators in the stochastic block model. *Electronic Journal of Statistics* **6**, 1847–1899. Publisher: Institute of Mathematical Statistics and Bernoulli Society.

CHAGANTY, N. R. & JOE, H. (2006). Range of correlation matrices for dependent Bernoulli random variables. *Biometrika* **93**, 197–206. Publisher: Oxford University Press.

CHANDNA, S., JANSON, S. & OLHEDE, S. C. (2022a). Edge coherence in multiplex networks. ArXiv:2202.09326 [math, stat].

CHANDNA, S. & MAUGIS, P.-A. (2020). Nonparametric regression for multiple heterogeneous networks. ArXiv:2001.04938 [stat].

CHANDNA, S., OLHEDE, S. C. & WOLFE, P. J. (2022b). Local linear graphon estimation using covariates. *Biometrika* **109**, 721–734.

DIACONIS, P. & JANSON, S. (2007). Graph limits and exchangeable random graphs. ArXiv:0712.2749 [math].

DONIER-MEROZ, E., DALALYAN, A. S., KRAMARZ, F., CHONÉ, P. & D'HAULTFOEUILLE, X. (2023). Graphon Estimation in bipartite graphs with observable edge labels and unobservable node labels. ArXiv:2304.03590 [cs, math, stat].

DUFOUR, C. & GRAINGER, J. (2023). NetworkHistogram.jl.

FISHKIND, D. E., ATHREYA, A., MENG, L., LYZINSKI, V. & PRIEBE, C. E. (2021). On a complete and sufficient statistic for the correlated Bernoulli random graph model. *Electronic Journal of Statistics* **15**, 2336–2359. Publisher: Institute of Mathematical Statistics and Bernoulli Society.

GAO, C., LU, Y., MA, Z. & ZHOU, H. H. (2016). Optimal estimation and completion of matrices with biclustering structures. *Journal of Machine Learning Research* **17**, 1–29.

GAO, C., LU, Y. & ZHOU, H. H. (2015). Rate-Optimal Graphon Estimation. *The Annals of Statistics* **43**, 2624–2652. Publisher: Institute of Mathematical Statistics.

GAUCHER, S. & KLOPP, O. (2021a). Maximum likelihood estimation of sparse networks with missing observations. *Journal of Statistical Planning and Inference* **215**, 299–329.

GAUCHER, S. & KLOPP, O. (2021b). Optimality of variational inference for stochasticblock model with missing links. In *Advances in Neural Information Processing Systems*, vol. 34. Curran Associates, Inc.

HALU, A., DE DOMENICO, M., ARENAS, A. & SHARMA, A. (2019). The multiplex network of human diseases. *npj Systems Biology and Applications* **5**, 1–12. Publisher: Nature Publishing Group.

HOOVER, D. N. (1979). Relations on Probability Spaces and Arrays of Random Variables. *Preprint, Institute for Advanced Study, Princeton* .

JANSON, S. & OLHEDE, S. (2021). Can smooth graphons in several dimensions be represented by smooth graphons on [0,1]. *Examples and Counterexamples* **1**, 100011.

KALLENBERG, O. (2005). *Probabilistic Symmetries and Invariance Principles*. Probability and Its Applications. New York: Springer-Verlag.

KIVELÄ, M., ARENAS, A., BARTHELEMY, M., GLEESON, J. P., MORENO, Y. & PORTER, M. A. (2014). Multilayer networks. *Journal of Complex Networks* **2**, 203–271.

KLOPP, O., TSYBAKOV, A. B. & VERZELEN, N. (2017). Oracle inequalities for network models and sparse graphon estimation. *The Annals of Statistics* **45**, 316–354. Publisher: Institute of Mathematical Statistics.

KUNSZENTI-KOVÁCS, D., LOVÁSZ, L. & SZEGEDY, B. (2022). Multigraph limits, unbounded kernels, and Banach space decorated graphs. *Journal of Functional Analysis* **282**, 109284.

LOVÁSZ, L. (2012). *Large networks and graph limits*, vol. 60. American Mathematical Soc.

LOVÁSZ, L. & SZEGEDY, B. (2010). Limits of compact decorated graphs. ArXiv:1010.5155 [math].

LUBBERTS, Z., ATHREYA, A., PARK, Y. & PRIEBE, C. E. (2024). Random line graphs and edge-attributed network inference. ArXiv:2103.14726 [cs, stat].

MAGNANI, M., MICENKOVA, B. & ROSSI, L. (2013). Combinatorial Analysis of Multiple Networks. ArXiv:1303.4986 [physics].

MASTRANDREA, R., FOURNET, J. & BARRAT, A. (2015). Contact Patterns in a High School: A Comparison between Data Collected Using Wearable Sensors, Contact Diaries and Friendship Surveys. *PLOS ONE* **10**, e0136497. Publisher: Public Library of Science.

OLHEDE, S. C. & WOLFE, P. J. (2014). Network histograms and universality of blockmodel approximation. *Proceedings of the National Academy of Sciences* **111**, 14722–14727. Publisher: Proceedings of the National Academy of Sciences.

PENSKY, M. (2019). Dynamic Network Models and Graphon Estimation. *The Annals of Statistics* **47**, 2378–2403. Publisher: Institute of Mathematical Statistics.

PENSKY, M. (2024). Signed Diverse Multiplex Networks: Clustering and Inference. ArXiv:2402.10242 [cs, stat].

POLLARD, D. (1990). *Empirical Processes: Theory and Applications*. NSF-CBMS Regional Conference Series in Probability and Statistics. Haywood CA and Alexandria VA: Institute of Mathematical Statistics and American Statistical Association.

RESNICK, M. D., BEARMAN, P. S., BLUM, R. W., BAUMAN, K. E., HARRIS, K. M., JONES, J., TABOR, J., BEUHRING, T., SIEVING, R. E., SHEW, M., IRELAND, M., BEARINGER, L. H. & UDRY, J. R. (1997). Protecting Adolescents From Harm: Findings From the National Longitudinal Study on Adolescent Health. *JAMA* **278**, 823–832.

SKEJA, A. & OLHEDE, S. C. (2024). Quantifying Multivariate Graph Dependencies: Theory and Estimation for Multiplex Graphs. ArXiv:2405.14482 [cs, math, stat].

SU, Y., WONG, R. K. W. & LEE, T. C. M. (2020). Network Estimation via Graphon With Node Features. *IEEE Transactions on Network Science and Engineering* **7**, 2078–2089. Conference Name: IEEE Transactions on Network Science and Engineering.

TEUGELS, J. L. (1990). Some representations of the multivariate Bernoulli and binomial distributions. *Journal of Multivariate Analysis* **32**, 256–268.

TSYBAKOV, A. B. (2009). *Introduction to Nonparametric Estimation*. Springer Series in Statistics. New York, NY: Springer.

VERDEYME, A. & OLHEDE, S. C. (2024). Hybrid of node and link communities for graphon estimation. ArXiv:2401.05088 [math, stat].

VERSHYNIN, R. (2011). Introduction to the non-asymptotic analysis of random matrices. ArXiv:1011.3027 [cs, math].

WANG, F., LI, W., PADILLA, O. H. M., YU, Y. & RINALDO, A. (2024). Multilayer random dot product graphs: Estimation and online change point detection. ArXiv:2306.15286 [stat].

WOLFE, P. J. & OLHEDE, S. C. (2013). Nonparametric graphon estimation. ArXiv:1309.5936 [math, stat].

XU, M., JOG, V. & LOH, P.-L. (2020). Optimal Rates for Community Estimation in the Weighted Stochastic Block Model. *The Annals of Statistics* **48**, 183–204. Publisher: Institute of Mathematical Statistics.

ZUCAL, G. (2024). Probability graphons: the right convergence point of view. ArXiv:2407.05998 [math].

D   Supplemental Material

D.1   Proofs of the main theorems

The proofs follow a similar argument as in Verdeyme & Olhede (2024) based on results and ideas from Gao et al. (2016); Klopp et al. (2017). The main difficulty resides in the dependence between the entries of $\boldsymbol{X}_{ij}$.

Remark D.1 *For fixed $i, j \in [n]$, $\boldsymbol{X}_{ij}^{(l)}$ is not independent from $\boldsymbol{X}_{ij}^{(k)}$, even conditionally on the latent variables $\{\xi_i\}_{i \in [n]}$. This dependence structure prevents us from using the same concentration bounds as in previous work, and we show here how we adapted them.*

D.1.1   Notation

Sometimes, we write $\|\cdot\|$ instead of $\|.\|_F$ for brevity but always mean the Frobenius inner product or norm unless specified otherwise. We remind readers of the notation and objects defined in Verdeyme & Olhede (2024).

Let $\mathcal{Z}_{n,s,k}$ be the mappings of $[n]$ to $[s]$ that can be written as $z(x, y) = u_s(u_k(x), u_k(y))$, with $u_s : [k]^2 \mapsto s$ and $u_k : [n] \mapsto [k]$ surjective mappings. This defines a clustering of edges in the region that are the union of blocks. Unless necessary, we will drop the resolution subscript (the size of the blocks) k and work with $\mathcal{Z}_{n,s}$. It can be shown that $|\mathcal{Z}_{n,s}| \leq \max(k, s)^n$ (Verdeyme & Olhede, 2024).

The operator z allows us to define the set of $n \times n$ parameter matrices from a (s, k)-stochastic shape model $\Theta_{s,k} = \left\{\{\boldsymbol{\theta}_{ij}\} : \boldsymbol{\theta}_{ij} = f(\xi_i, \xi_j); f \text{ specified as in definition 3.1 of the main paper}\right\}$ in another way:

$$\Theta_{s,k} = \left\{\{\boldsymbol{\theta}_{ij}\} : \boldsymbol{\theta}_{ij} = Q_{z(i,j)}; z \in \mathcal{Z}_{n,s,k}\right\}.$$

Given $\eta \in \mathbb{R}^{n \times n \times L}$, we let

$$\bar{\eta}_c(z) = \frac{1}{|z^{-1}(c)|} \sum_{i,j:z(i,j)=c} \eta_{ij} \in \mathbb{R}^L,$$

where $z^{-1}(c) = \{i, j \in [n] \text{ such that } z(i, j) = c\}$. This defines a shape average based on the shape assignment indicated by z. It can be shown that finding $\widehat{\boldsymbol{\theta}}$ as defined in eq. (3) in the main paper is equivalent to finding $\hat{z}$ and setting $\widehat{\boldsymbol{\theta}} = \bar{\boldsymbol{X}}(\hat{z})$ (Wolfe & Olhede, 2013; Gao et al., 2016; Verdeyme & Olhede, 2024).

Remark D.2 *We remind the reader that the $(\binom{k}{2}, k)$-stochastic shape model is equivalent to the traditional stochastic block model with k blocks.*

D.1.2   Proof of Theorem 4.1, stochastic shape model assumption

In this case, we denote the true value of each shape by $Q_c^* \in [0, 1]^{s \times L}$ and the oracle assignment by $z^* \in \mathcal{Z}_{n,s}$ such that $\boldsymbol{\theta}_{ij} = Q_{z(i,j)}^*$ for any $i \neq j$. For these estimated $\hat{z}$, we define $\tilde{Q}_c \in [0, 1]^{s \times L}$ by $\tilde{Q}_c = \bar{\boldsymbol{\theta}}_c(\hat{z})$, and $\widetilde{\boldsymbol{\theta}}_{ij} = \tilde{Q}_{\hat{z}(i,j)}$ for any $i \neq j$. The diagonal elements of $\widetilde{\boldsymbol{\theta}}$ are set to the probability distribution on $\mathcal{K}$ that puts all its mass at the zero element.

Proof D.1 (of theorem 4.1) *This proof follows a similar argument to the one used by (Gao et al., 2016) and Verdeyme & Olhede (2024). By definition of our estimator, we have $\|\widehat{\boldsymbol{\theta}} - \boldsymbol{X}\|_F^2 \leq \|\boldsymbol{\theta} - \boldsymbol{X}\|_F^2$, which implies*

$$\|\widehat{\boldsymbol{\theta}} - \boldsymbol{\theta}\|_F^2 \leq 2\langle \widehat{\boldsymbol{\theta}} - \boldsymbol{\theta}, \boldsymbol{X} - \boldsymbol{\theta}\rangle,$$

which can be further bounded by

$$\|\widehat{\boldsymbol{\theta}} - \boldsymbol{\theta}\|^2 \leq 2\|\widehat{\boldsymbol{\theta}} - \widetilde{\boldsymbol{\theta}}\| \left|\left\langle \frac{\widehat{\boldsymbol{\theta}} - \widetilde{\boldsymbol{\theta}}}{\|\widehat{\boldsymbol{\theta}} - \widetilde{\boldsymbol{\theta}}\|}, \boldsymbol{X} - \boldsymbol{\theta}\right\rangle\right| + 2\left(\|\widehat{\boldsymbol{\theta}} - \widetilde{\boldsymbol{\theta}}\| + \|\widetilde{\boldsymbol{\theta}} - \boldsymbol{\theta}\|\right) \left|\left\langle \frac{\widetilde{\boldsymbol{\theta}} - \boldsymbol{\theta}}{\|\widetilde{\boldsymbol{\theta}} - \boldsymbol{\theta}\|}, \boldsymbol{X} - \boldsymbol{\theta}\right\rangle\right|. \tag{6}$$

Lemmas D.2 to D.4 show that for any $C' > 0$, there exists a $C > 0$ such that all of the following three terms

$$\underbrace{\|\widehat{\boldsymbol{\theta}} - \widetilde{\boldsymbol{\theta}}\|}_{\text{Lemma D.4}}, \quad \underbrace{\left|\left\langle \frac{\widehat{\boldsymbol{\theta}} - \widetilde{\boldsymbol{\theta}}}{\|\widehat{\boldsymbol{\theta}} - \widetilde{\boldsymbol{\theta}}\|}, \boldsymbol{X} - \boldsymbol{\theta}\right\rangle\right|}_{\text{Lemma D.2}}, \quad \underbrace{\left|\left\langle \frac{\widetilde{\boldsymbol{\theta}} - \boldsymbol{\theta}}{\|\widetilde{\boldsymbol{\theta}} - \boldsymbol{\theta}\|}, \boldsymbol{X} - \boldsymbol{\theta}\right\rangle\right|}_{\text{Lemma D.3}},$$

are bounded by $C\sqrt{Ls + n\log(\max(k,s))}$ with probability at least $1 - 3\exp\left(-C'n\log(\max(k,s))\right)$. Combining this bound with eq. (6), we obtain

$$\|\widehat{\boldsymbol{\theta}} - \boldsymbol{\theta}\|^2 \le 2C\|\widehat{\boldsymbol{\theta}} - \boldsymbol{\theta}\|\sqrt{Ls + n\log(\max(k,s))} + 4C^2\left(Ls + n\log(\max(k,s))\right).$$

Solving for $\|\widehat{\boldsymbol{\theta}} - \boldsymbol{\theta}\|$ and setting $C_1 = (1 + \sqrt{5})C$, we get

$$\|\widehat{\boldsymbol{\theta}} - \boldsymbol{\theta}\| \le C_1\sqrt{Ls + n\log(\max(k,s))},$$

with probability at least $1 - 3\exp\left(-C'n\log(\max(k,s))\right)$. To get the bound in expectation, let $\varepsilon^2 = C_1\left(Ls/n^2 + \log(\max(k,s))/n\right)$, we have

$$\begin{aligned}
\mathbb{E}\left[n^{-2}\|\widehat{\boldsymbol{\theta}} - \boldsymbol{\theta}\|^2\right] &= \mathbb{E}\left[n^{-2}\|\widehat{\boldsymbol{\theta}} - \boldsymbol{\theta}\|^2 1_{\{n^{-2}\|\widehat{\boldsymbol{\theta}} - \boldsymbol{\theta}\|^2 \le \varepsilon^2\}}\right] + \mathbb{E}\left[n^{-2}\|\widehat{\boldsymbol{\theta}} - \boldsymbol{\theta}\|^2 1_{\{n^{-2}\|\widehat{\boldsymbol{\theta}} - \boldsymbol{\theta}\|^2 > \varepsilon^2\}}\right] \\
&\le \varepsilon^2 + \mathrm{pr}\left(n^{-2}\|\widehat{\boldsymbol{\theta}} - \boldsymbol{\theta}\|^2 > \varepsilon^2\right) \\
&\le \varepsilon^2 + 3\exp\left(-C'n\log(\max(k,s))\right) \\
&\le C_1\left(\frac{Ls}{n^2} + \frac{\log(\max(k,s))}{n}\right) + 3\exp\left(-C'n\log(\max(k,s))\right).
\end{aligned}$$

Since ε^2 is the dominating term, this concludes the proof.

D.1.3 Proof of Theorem B.1: Holder assumption

We recall the result from Verdeyme & Olhede (2024, Lemma 3.1).

Lemma D.1 *Under assumptions 1 and 2, there exists $z^* \in \mathcal{Z}_{n,s}$ and a constant $\beta \ge 1$ such that $D_{z^*} \propto s^{-\beta/2}$ and*

$$\frac{1}{n^2}\|\boldsymbol{\theta} - \overline{\boldsymbol{\theta}}(z^*)\|_F^2 \le CM^2 s^{-\beta(\alpha \wedge 1)},$$

holds for some universal constant $C > 0$.

Remark D.3 (On lemma D.1) *Since the stochastic block model with k blocks is a specific instance of a $SSM(s,k)$, we have the upper bound from (Gao et al., 2016, Lemma 2.1) with $\beta = 1$. This is equivalent to no smoothing on the blocks; the bigger the β, the more smoothing was done.*

We need to redefine z^* and Q^*. We choose z^* as the one from lemma D.1, and we define $Q_c^* = \overline{\boldsymbol{\theta}}_c(z^*)$, and $\boldsymbol{\theta}_{ij}^* = Q_{z(i,j)}^*$ for $i \ne j$ and $\boldsymbol{\theta}_{ii}^* = \delta_{0_\mathcal{K}}$ representing the probability distribution on $\mathcal{K}$ that puts all its mass at the zero element.

Proof D.2 (of theorem B.1) *The proof follows Verdeyme & Olhede (2024, Proof of Theorem 3.3). We only detail the last step for choosing δ such that $s = n^\delta$. Following the proof previously mentioned, we get that for all $C' > 0$, there exists $C_1 > 0$ such that*

$$\frac{1}{n^2}\|\widehat{\boldsymbol{\theta}} - \boldsymbol{\theta}\|_F^2 \le C\left(s^{-\beta(\alpha \wedge 1)} + \frac{Ls}{n^2} + \frac{\log(\max(k,s))}{n}\right), \tag{7}$$

with probability at least $1 - \exp(-C'n)$. Following Verdeyme & Olhede (2024); Gao et al. (2015), let $s = s(n) = n^\delta$ with $\delta = 2\beta^{-1}/(\alpha + 1)$. Plugging that choice back in eq. (7) leads to

$$\frac{1}{n^2}\|\widehat{\boldsymbol{\theta}} - \boldsymbol{\theta}\|_F^2 \le C\left(n^{-2\alpha/(\alpha+1)} + Ln^{-2(1-\beta^{-1})/(\alpha+1)} + \log(n)/n\right).$$

We get two different upper bounds depending on the β from lemma D.1, but with the constant independent of L. If $\beta \ge 2/\left(2 - (1 + \alpha \wedge 1)\log_n(L)\right) > 1$, we get

$$\frac{1}{n^2}\|\widehat{\boldsymbol{\theta}} - \boldsymbol{\theta}\|_F^2 \le C_1\left(n^{-2\alpha/(\alpha+1)} + \log(n)/n\right),$$

with C_1 independent of L. As noted in remark D.3, the more smoothing the oracle estimator can perform, the sooner this condition will be satisfied (as $2/\left(2 - (1 + \alpha \wedge 1)\log_n(L)\right) \to 1$ as $n \to \infty$). Otherwise, we have $\beta > 1$ leading to

$$\frac{1}{n^2}\|\widehat{\boldsymbol{\theta}} - \boldsymbol{\theta}\|_F^2 \le C_2\left(Ln^{-2\alpha/(\alpha+1)} + \log(n)/n\right), \tag{8}$$

where both C_2 is independent of L. In both cases, eq. (8) holds.

D.2   Oracle inequalities

Lemma D.2 *For any constant $C' > 0$, there exists a constant $C > 0$ only depending on C' such that*

$$\left|\left\langle \frac{\widehat{\boldsymbol{\theta}} - \widetilde{\boldsymbol{\theta}}}{\|\widehat{\boldsymbol{\theta}} - \widetilde{\boldsymbol{\theta}}\|}, \boldsymbol{X} - \boldsymbol{\theta} \right\rangle_F \right| \leq C\sqrt{Ls + n\log(\max(k,s))},$$

with probability at least $1 - \exp\left(-C'n\log(\max(k,s))\right)$.

Proof D.3 (of lemma D.2) *For each $z \in \mathcal{Z}_{n,s}$, define the set $\mathcal{B}_z$ by $\mathcal{B}_z = \left\{\{a_{ij}\} : a_{ijl} = Q_{cl} \text{ if } (i,j) \in z^{-1}(c) \text{ for some } Q_{cl}, \text{ and } \sum_{ijl} a_{ijl}^2 \leq 1\right\}$. In other words, $\mathcal{B}_z$ collects the element of $\mathcal{B}$ as defined in lemma D.5 determined by w. We then get*

$$\left|\left\langle \frac{\widehat{\boldsymbol{\theta}} - \widetilde{\boldsymbol{\theta}}}{\|\widehat{\boldsymbol{\theta}} - \widetilde{\boldsymbol{\theta}}\|}, \boldsymbol{X} - \boldsymbol{\theta} \right\rangle_F \right| \leq \max_{z \in \mathcal{Z}_{n,s}} \sup_{a \in \mathcal{B}_z} \left| \sum_l \sum_{ij} a_{ijl} \left(\boldsymbol{X}_{ij}^{(l)} - \boldsymbol{\theta}_{ij}^{(l)} \right) \right|.$$

Using a union bound argument and lemma D.5, we get

$$\mathrm{pr}\left(\max_{z \in \mathcal{Z}_{n,s}} \sup_{a \in \mathcal{B}_z} \left| \sum_l \sum_{ij} a_{ijl} \left(\boldsymbol{X}_{ij}^{(l)} - \boldsymbol{\theta}_{ij}^{(l)} \right) \right| > t \right) \leq \sum_{z \in \mathcal{Z}_{n,s}} \mathcal{N}\left(1/2, \mathcal{B}_z, \|\cdot\|\right) \exp(-t^2/8).$$

Since $\mathcal{B}_z$ has $(L-1)s$ degree of freedom, a standard bound for covering numbers implies $\mathcal{N}\left(1/2, \mathcal{B}_z, \|\cdot\|\right) \leq \exp(C_1 Ls)$ (Pollard, 1990, Lemma 4.1). Using $|\mathcal{Z}_{n,s}| < \exp(n\log(\max(k,s)))$, we get

$$\mathrm{pr}\left(\max_{z \in \mathcal{Z}_{n,s}} \sup_{a \in \mathcal{B}_z} \left| \sum_l \sum_{ij} a_{ijl} \left(\boldsymbol{X}_{ij}^{(l)} - \boldsymbol{\theta}_{ij}^{(l)} \right) \right| > t \right) \leq \exp\left(-t^2/8 + C_1 Ls + n\log(\max(k,s)) \right).$$

Picking $t^2 \propto Ls + n\log(\max(k,s))$ finishes the proof.

Lemma D.3 *For any constant $C' > 0$, there exists a constant $C > 0$ only depending on C', such that*

$$\left|\left\langle \frac{\widetilde{\boldsymbol{\theta}} - \boldsymbol{\theta}}{\|\widetilde{\boldsymbol{\theta}} - \boldsymbol{\theta}\|}, \boldsymbol{X} - \boldsymbol{\theta} \right\rangle_F \right| \leq C\sqrt{n\log(\max(k,s))},$$

with probability at least $1 - \exp\left(-C'n\log(\max(k,s))\right)$.

Proof D.4 (of lemma D.3) *Follows by using a union bound argument on $\mathcal{Z}_{n,s}$ and lemma D.5 (as in the proof of lemma D.2).*

Lemma D.4 *For any constant $C' > 0$, there exists a constant $C > 0$ only depending on C', such that*

$$\|\widehat{\boldsymbol{\theta}} - \widetilde{\boldsymbol{\theta}}\|_F \leq C\sqrt{Ls + n\log(\max(k,s))}$$

with probability at least $1 - \exp{-C'n\log(\max(k,s))}$.

Proof D.5 (of lemma D.4)

$$\begin{aligned}
\|\widehat{\boldsymbol{\theta}} - \widetilde{\boldsymbol{\theta}}\|_F &= \sum_{l=1}^L \|\widehat{\boldsymbol{\theta}}^{(l)} - \widetilde{\boldsymbol{\theta}}^{(l)}\|_2^2 \\
&= \sum_{l=1}^L \sum_{i,j=1}^n \left(\widehat{\boldsymbol{\theta}}_{ij}^{(l)} - \widetilde{\boldsymbol{\theta}}_{ij}^{(l)} \right)^2 \\
&= \sum_{c \in [S]} \sum_{l=1}^L |\widehat{z}^{-1}(c)| \left(\overline{\boldsymbol{X}}_c^{(l)}(\widehat{z}) - \overline{\boldsymbol{\theta}}_c^{(l)}(\widehat{z}) \right)^2 \\
&\leq \max_{z \in \mathcal{Z}_{n,s}} \sum_{c \in [S]} \sum_{l=1}^l |z^{-1}(c)| \left(\overline{\boldsymbol{X}}_c^{(l)}(z) - \overline{\boldsymbol{\theta}}_c^{(l)}(z) \right)^2
\end{aligned}$$

For a given $z \in \mathcal{Z}_{n,s}$, let $n_c = |z^{-1}(c)|$ and define

$$V_c(z) = \frac{1}{n_c} \sum_l \left(\sum_{(i,j) \in z^{-1}(c)} \left(\mathbf{X}_{ij}^{(l)} - \boldsymbol{\theta}_{ij}^{(l)} \right) \right)^2.$$

We then have

$$\|\widehat{\boldsymbol{\theta}} - \widetilde{\boldsymbol{\theta}}\|_F \le \max_{z \in \mathcal{Z}_{n,s}} \sum_{c \in [s]} \mathbb{E}\left[V_c(z)\right] + \max_{z \in \mathcal{Z}_{n,s}} \sum_{c \in [s]} \left(V_c(z) - \mathbb{E}\left[V_c(z)\right] \right).$$

We bound the first term:

$$\begin{aligned}
\mathbb{E}\left[V_c(z)\right] &= \mathbb{E}\left[\frac{1}{n_c} \sum_l \left(\sum_{(i,j) \in z^{-1}(c)} \left(\mathbf{X}_{ij}^{(l)} - \boldsymbol{\theta}_{ij}^{(l)} \right) \right)^2 \right] \\
&= \frac{1}{n_c} \sum_l \mathbb{E}\left[\left(\sum_{(i,j) \in z^{-1}(c)} \left(\mathbf{X}_{ij}^{(l)} - \boldsymbol{\theta}_{ij}^{(l)} \right) \right)^2 \right] \\
&= \frac{1}{n_c} \sum_l \sum_{(i,j) \in z^{-1}(c)} \mathrm{var}\left(\mathbf{X}_{ij}^{(l)} \right) \\
&\le L,
\end{aligned}$$

as for a fixed l, the variables $\mathbf{X}_{ij}^{(l)}$ and $\mathbf{X}_{qr}^{(l)}$ are independent for all $(q,r) \ne (i,j)$ and $(q,r) \ne (j,i)$, and $\mathrm{var}\left(\mathbf{X}_{ij}^{(l)} \right) \le 1$.

We now show that for a fixed w, $V_c(z)$ is a sub-exponential random variable with constant sub-exponential parameter. This will allow us to finish the proof as in Verdeyme & Olhede (2024), replacing the upper bound of $\mathbb{E}\left[V_c(z)\right]$ by the one computed above. We first have

$$V_c(z) \le \frac{1}{n_c} \sum_l \left(\sum_{(i,j) \in z^{-1}(c)} \left| \mathbf{X}_{ij}^{(l)} - \boldsymbol{\theta}_{ij}^{(l)} \right| \right)^2 \le \frac{1}{n_c} \left(\sum_l \sum_{(i,j) \in z^{-1}(c)} \left| \mathbf{X}_{ij}^{(l)} - \boldsymbol{\theta}_{ij}^{(l)} \right| \right)^2.$$

We then have, for any $t > 0$

$$\begin{aligned}
\mathrm{pr}\left(V_c(z) > t\right) &\le \mathrm{pr}\left(\frac{1}{n_c} \left(\sum_l \sum_{(i,j) \in z^{-1}(c)} \left| \mathbf{X}_{ij}^{(l)} - \boldsymbol{\theta}_{ij}^{(l)} \right| \right)^2 > t \right) \\
&= \mathrm{pr}\left(\sum_l \sum_{(i,j) \in z^{-1}(c)} \left| \mathbf{X}_{ij}^{(l)} - \boldsymbol{\theta}_{ij}^{(l)} \right| > \sqrt{t n_c} \right) \\
&= \mathrm{pr}\left(\sum_{(i,j) \in z^{-1}(c)} \left\| \mathbf{X}_{ij} - \boldsymbol{\theta}_{ij} \right\|_1 > \sqrt{t n_c} \right).
\end{aligned}$$

Since $\left\| \mathbf{X}_{ij} - \boldsymbol{\theta}_{ij} \right\|_1 \le \|\mathbf{X}_{ij}\|_1 + \|\boldsymbol{\theta}_{ij}\|_1 = 2$, we get that $\left\| \mathbf{X}_{ij} - \boldsymbol{\theta}_{ij} \right\|_1$ is a sub-gaussian random variable. Using Hoeffding's inequality for sub-gaussian variable (Vershynin, 2011, Prop. 5.10), we have

$$\mathrm{pr}\left(V_c(z) > t\right) \le \exp\left(1 - C \frac{t n_c}{4 n_c} \right) \le \exp\left(1 - C t / 4 \right)$$

for some universal constant $C > 0$.

The proof then concludes exactly as in Verdeyme & Olhede (2024, proof of Lemma A.4) replacing s by sL in the upper bound of $\sum_c \mathbb{E}\left[V_c(z)\right]$.

D.2.1 Auxiliary result

Lemma D.5 *Let $\mathcal{B} \subset \left\{a \in \mathbb{R}^{n \times n \times L} : \|a\|_F \leq 1\right\}$. Then for any $a \in \mathcal{B}$ we have*

$$\mathrm{pr}\left(\left|\sum_l \sum_{ij} a_{ijl}\left(\boldsymbol{X}_{ij}^{(l)} - \boldsymbol{\theta}_{ij}^{(l)}\right)\right| > t\right) \leq \exp\left(-t^2/8\right).$$

If we additionally suppose that $\mathcal{B}$ is such that for any $a, b \in \mathcal{B}$

$$\frac{a-b}{\|a-b\|_F} \in \mathcal{B}, \tag{9}$$

we then have

$$\mathrm{pr}\left(\sup_{a \in \mathcal{B}}\left|\sum_l \sum_{ij} a_{ijl}\left(\boldsymbol{X}_{ij}^{(l)} - \boldsymbol{\theta}_{ij}^{(l)}\right)\right| > t\right) \leq \mathcal{N}(1/2, \mathcal{B}, \|\cdot\|)\exp\left(-Ct^2/32\right).$$

Proof D.6 (of lemma D.5) *The proof follows Verdeyme & Olhede (2024, Lemma A.1); the only difference is using McDiarmid's inequality instead of Hoeffding's, but we repeat the whole proof. Let us first notice that*

$$\left|\sum_l \sum_{ij} a_{ijl}\left(\boldsymbol{X}_{ij}^{(l)} - \boldsymbol{\theta}_{ij}^{(l)}\right)\right| = |\langle a, \boldsymbol{X} - \boldsymbol{\theta}\rangle|.$$

We will show that for each $b \in \mathcal{B}$, $\langle b, \boldsymbol{X} - \boldsymbol{\theta}\rangle$ is a function of $\{\boldsymbol{X}_{ij}\}_{i > j}$ that satisfies the bounded difference properties.

$$\langle b, \boldsymbol{X} - \boldsymbol{\theta}\rangle = \sum_l \sum_{ij} b_{ijl}\left(\boldsymbol{X}_{ij}^{(l)} - \boldsymbol{\theta}_{ij}^{(l)}\right) = \sum_{ij}\langle b_{ij}, \boldsymbol{X}_{ij}\rangle - 2\sum_{ij}\langle b_{ij}, \boldsymbol{\theta}_{ij}\rangle,$$

where $b_{ij} = (b_{ij1}, \ldots, b_{ijL})$. Let's examine what happens when we change the value of this function's (k, l)th coordinate. $\boldsymbol{X}_{kl}$ is a binary vector with exactly one non-zero component $r \in [L]$. Its contribution to the function value is $b_{ijr} + b_{jir}$. Changing the value of $\boldsymbol{X}_{kl}$ will then change this contribution to $b_{ijq} + b_{jiq}$ for a $q \in [L]$. The absolute value of the difference is then

$$|b_{ijr} + b_{jir} - b_{ijq} - b_{jiq}| \leq 4\max_l |b_{ijl}|.$$

Notice that $\mathbb{E}\left[\langle b, \boldsymbol{X} - \boldsymbol{\theta}\rangle\right] = 0$. Using the bounded difference property we have just shown, we use McDiarmid's inequality to get

$$\mathrm{pr}\left(|\langle b, \boldsymbol{X} - \boldsymbol{\theta}\rangle| \geq \epsilon\right) \leq \exp\left(-\frac{2\epsilon^2}{16\sum_{ij}\max_l(b_{ijl})^2}\right) \leq \exp\left(-\frac{\epsilon^2}{8}\right), \tag{10}$$

since $\sum_{ij}\max_l(b_{ijl})^2 \leq \sum_{ijl}(b_{ijl})^2 = \|b\|_F^2 \leq 1$. This shows the first part of the proposition.

Let $\mathcal{B}'$ be a $1/2$-net of $\mathcal{B}$ such that $|\mathcal{B}'| \leq \mathcal{N}(1/2, \mathcal{B}, \|\cdot\|)$. For any $a \in \mathcal{B}$ there is a $b \in \mathcal{B}'$ such that $\|a - b\| \leq 1/2$.

Thus,

$$|\langle a, \boldsymbol{X} - \boldsymbol{\theta}\rangle| \leq |\langle a - b, \boldsymbol{X} - \boldsymbol{\theta}\rangle| + |\langle b, \boldsymbol{X} - \boldsymbol{\theta}\rangle|$$

$$\leq \|a - b\|\left|\left\langle \frac{a-b}{\|a-b\|}, \boldsymbol{X} - \boldsymbol{\theta}\right\rangle\right| + |\langle b, \boldsymbol{X} - \boldsymbol{\theta}\rangle|$$

$$\leq \frac{1}{2}\sup_{a \in \mathcal{B}}|\langle a, \boldsymbol{X} - \boldsymbol{\theta}\rangle| + |\langle b, \boldsymbol{X} - \boldsymbol{\theta}\rangle|,$$

where the last inequality follows from the assumption eq. (9). Taking the supremum with respect to $\mathcal{B}$ and maximum with respect to $\mathcal{B}'$ on both sides, we have

$$\sup_{a \in \mathcal{B}}|\langle a, \boldsymbol{X} - \boldsymbol{\theta}\rangle| \leq 2\max_{b \in \mathcal{B}'}|\langle b, \boldsymbol{X} - \boldsymbol{\theta}\rangle|.$$

We then get

$$\mathrm{pr}\left(\sup_{a \subset \mathcal{B}}|\langle a, \boldsymbol{X} - \boldsymbol{\theta}\rangle| \geq t\right) \leq \mathrm{pr}\left(2\max_{b \in \mathcal{B}'}|\langle b, \boldsymbol{X} - \boldsymbol{\theta}\rangle| \geq t\right)$$

$$\leq \sum_{b \in \mathcal{B}'}\mathrm{pr}\left(|\langle b, \boldsymbol{X} - \boldsymbol{\theta}\rangle| \geq \frac{t}{2}\right).$$

Combining what we have with eq. (10), we get

$$\mathrm{pr}\left(\sup_{a \in \mathcal{B}} |\langle a, \boldsymbol{X} - \boldsymbol{\theta}\rangle| > t\right) \leq \sum_{b \in \mathcal{B}'} \exp\left(-t^2/32\right)$$

$$= |\mathcal{B}'| \exp\left(-t^2/32\right)$$

$$\leq \mathcal{N}(1/2, \mathcal{B}, \|\cdot\|) \exp\left(-t^2/32\right),$$

which concludes the proof.

D.3   Additional experimental results
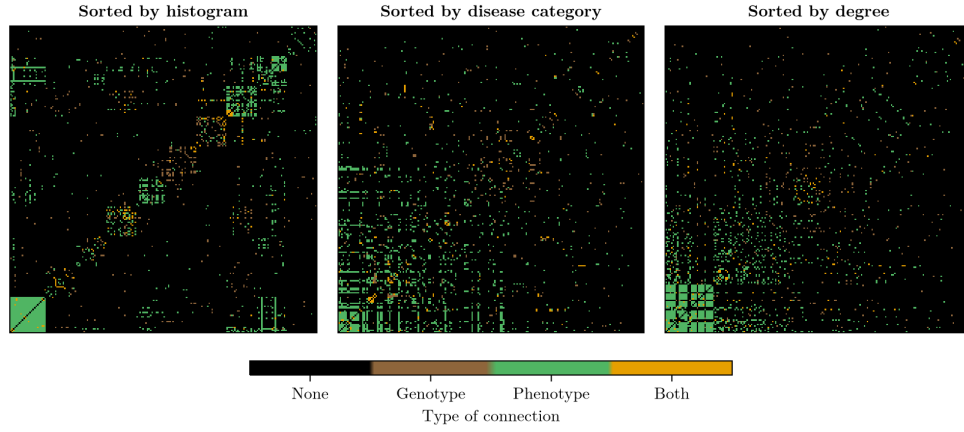
D.3.1   Multiplex of human diseases

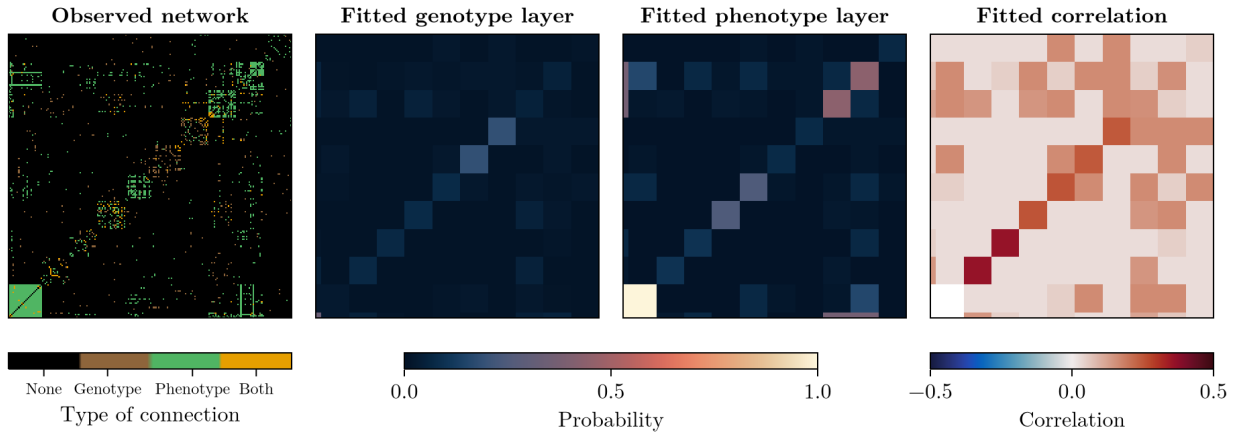Figure 7: Different ordering of the multiplex network of human diseases reveals different structures.

Figure 8: Fitted estimator to the multiplex of human diseases.

Community	Diseases
1	Charcot-Marie-Tooth disease type X, combined oxidative phosphorylation deficiency, hereditary spastic paraplegia, spinocerebellar ataxia
2	Albright's hereditary osteodystrophy, Greig cephalopolysyndactyly syndrome, Larsen syndrome, Saethre-Chotzen syndrome, acromesomelic dysplasia, Hunter-Thompson type, congenital disorder of glycosylation, congenital disorder of glycosylation type II, congenital muscular dystrophy, craniosynostosis, cutis laxa, erythrokeratodermia variabilis, hemolytic-uremic syndrome, lissencephaly, microphthalmia, olivopontocerebellar atrophy, piebaldism, popliteal pterygium syndrome, pseudohypoparathyroidism, pseudopseudohypoparathyroidism, syndromic X-linked intellectual disability
3	Frasier syndrome, Gerstmann-Straussler-Scheinker syndrome, Kaposi's sarcoma, Pick's disease, Rett syndrome, X-linked hypophosphatemia, amyotrophic lateral sclerosis, amyotrophic lateral sclerosis type 1, amyotrophic lateral sclerosis type 11, amyotrophic lateral sclerosis type 12, amyotrophic lateral sclerosis type 4, amyotrophic lateral sclerosis type 6, arterial calcification of infancy, episodic ataxia, familial hemiplegic migraine, familial partial lipodystrophy, fatal familial insomnia, obesity, oculocutaneous albinism, progressive supranuclear palsy
4	ACTH-secreting pituitary adenoma, Blau syndrome, Clouston syndrome, Klippel-Feil syndrome, Scheie syndrome, X-linked nonsyndromic deafness, atypical teratoid rhabdoid tumor, brachydactyly, homocystinuria, hypospadias, mucopolysaccharidosis, mucopolysaccharidosis I, multiple synostoses syndrome, nevoid basal cell carcinoma syndrome, oculodentodigital dysplasia, retinoblastoma, syndactyly, synpolydactyly, tarsal-carpal coalition syndrome, trilateral retinoblastoma
5	Andersen-Tawil syndrome, Becker muscular dystrophy, Brugada syndrome, Cockayne syndrome, Dravet Syndrome, Duchenne muscular dystrophy, Fukuyama congenital muscular dystrophy, Jervell-Lange Nielsen syndrome, Ohtahara syndrome, Robinow syndrome, Rothmund-Thomson syndrome, atrial heart septal defect, dilated cardiomyopathy, familial atrial fibrillation, hemochromatosis, hypertrophic cardiomyopathy, infantile epileptic encephalopathy, long QT syndrome, renal agenesis, scapuloperoneal myopathy
6	Fanconi's anemia, LEOPARD syndrome, Leigh disease, UV-sensitive syndrome, Walker-Warburg syndrome, acrodysostosis, atelosteogenesis, autosomal recessive non-syndromic intellectual disability, congenital hypothyroidism, fatal infantile encephalocardiomyopathy, holoprosencephaly, multiple epiphyseal dysplasia, multiple sclerosis, osteogenesis imperfecta, otospondylomegaepiphyseal dysplasia, pontocerebellar hypoplasia type 2A, pontocerebellar hypoplasia type 4, pre-eclampsia, severe congenital neutropenia, tooth agenesis
7	Antley-Bixler syndrome, Crouzon syndrome, LADD syndrome, Peutz-Jeghers syndrome, Pfeiffer syndrome, Rubinstein-Taybi syndrome, Stickler syndrome, achondrogenesis type IB, achondrogenesis type II, achondroplasia, acrocephalosyndactylia, cardiofaciocutaneous syndrome, colorectal cancer, fragile X syndrome, fragile X-associated tremor/ataxia syndrome, pilomatrixoma, seminoma, spondyloepiphyseal dysplasia congenita, testicular cancer, testicular germ cell cancer
8	Bannayan-Riley-Ruvalcaba syndrome, Bothnia retinal dystrophy, Cowden disease, Leber congenital amaurosis, Senior-Loken syndrome, Stargardt disease, Usher syndrome, VACTERL association, Waardenburg's syndrome, achromatopsia, age related macular degeneration, bestrophinopathy, cerebral amyloid angiopathy, congenital stationary night blindness, dysplastic nevus syndrome, familial meningioma, fundus albipunctatus, melanoma, retinitis pigmentosa, skin melanoma
9	Charcot-Marie-Tooth disease intermediate type, Charcot-Marie-Tooth disease type 1, Charcot-Marie-Tooth disease type 2, Charcot-Marie-Tooth disease type 4, Emery-Dreifuss muscular dystrophy, Parkinson's disease, autistic disorder, autosomal dominant nonsyndromic deafness, autosomal recessive nonsyndromic deafness, benign neonatal seizures, cone-rod dystrophy, distal hereditary motor neuropathy, distal muscular dystrophy, essential tremor, generalized epilepsy with febrile seizures plus, hypokalemic periodic paralysis, limb-girdle muscular dystrophy, nephronophthisis, nephrotic syndrome, thrombophilia
10	Aicardi-Goutieres syndrome, FG syndrome, Gaucher's disease, Joubert syndrome, Kallmann syndrome, Meckel syndrome, Noonan syndrome, Simpson-Golabi-Behmel syndrome, Weill-Marchesani syndrome, asphyxiating thoracic dystrophy, autosomal dominant non-syndromic intellectual disability, coenzyme Q10 deficiency disease, congenital disorder of glycosylation type I, congenital generalized lipodystrophy, congenital myasthenic syndrome, craniometaphyseal dysplasia, distal arthrogryposis, hereditary sensory neuropathy, muscular dystrophy-dystroglycanopathy, osteopetrosis
11	46 XY gonadal dysgenesis, Baller-Gerold syndrome, Beckwith-Wiedemann syndrome, Costello syndrome, Pallister-Hall syndrome, acute lymphocytic leukemia, azoospermia, celiac disease, esophagus squamous cell carcinoma, hyperkalemic periodic paralysis, hypohidrotic ectodermal dysplasia, orofacial cleft, primary ciliary dyskinesia, primary pigmented nodular adrenocortical disease, seborrheic keratosis, systemic lupus erythematosus, tetralogy of Fallot, thrombocytopenia, type 1 diabetes mellitus, xeroderma pigmentosum

Table 2: Community fitted in the multiplex network of human diseases

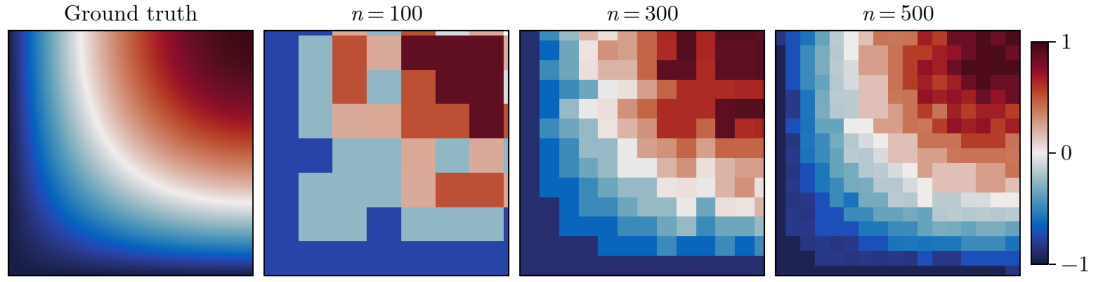# E   Additional simulation studies

Figure 9: Simulation with correlation between layers ranging from -1 to 1. Only the correlation layer is shown, as the marginal layers are around 0.5; this is due to the restrictions on admissible correlations (Chaganty & Joe, 2006).
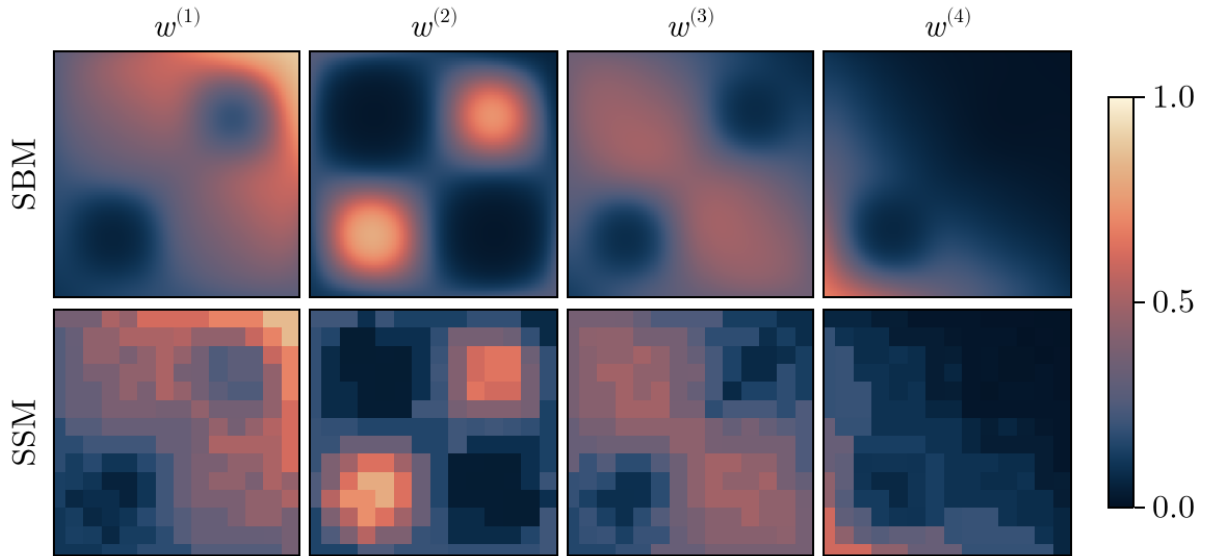

Figure 10: W_3 and SSM approximation based on a graph with 300 nodes.